International Journal for Multidisciplinary Research (IJFMR)
E-ISSN: 2582-2160 ● Website: www.ijfmr.com ● Email: editor@ijfmr.com

Microwave Hydrothermal Synthesis and Electrical Characterization of Zn-Doped $NiCo_2O_4$ Spinel Oxide

Satyanarayana Maheshwaram[1], Ravinder Reddy Butreddy[2], Ashok Bandi[3]

[1]Deapartment of Physics, Government Degree College- Rajendranagar
[2]Deapartment of Physics, Osmania University.
[3]Department of Physics, SRR Government College(A)- Karimnagar

ABSTRACT

Zn-doped nickel cobaltite ($NiCo_2-xZnxO_4$) nanoparticles with varying Zn concentrations were synthesized through a microwave-assisted hydrothermal method. The prepared samples were systematically characterized using X-ray diffraction (XRD), Fourier transform infrared spectroscopy (FTIR), X-ray photoelectron spectroscopy (XPS), scanning electron microscopy (SEM), and dielectric measurements. XRD analysis confirmed the formation of a single-phase cubic spinel structure without secondary impurity phases. FTIR studies revealed characteristic metal–oxygen vibrational bands associated with the spinel framework, while XPS analysis verified the oxidation states and successful incorporation of Zn ions into the $NiCo_2O_4$ lattice. The dielectric properties demonstrated strong frequency-dependent behavior, where the dielectric constant and dielectric loss decreased with increasing frequency due to interfacial polarization effects. AC conductivity increased progressively with frequency, indicating enhanced hopping conduction between mixed valence ions. The Zn-doped compositions exhibited improved electrical transport characteristics compared with un doped $NiCo_2O_4$. Among all compositions, the x = 0.08 sample showed superior conductivity and dielectric stability, suggesting its suitability for high-frequency electronic and energy-storage applications

Keywords: Zn-substituted $NiCo_2O_4$, spinel oxide nanoparticles, microwave hydrothermal synthesis, dielectric behavior, AC conductivity, dielectric loss, frequency response, nanomaterials, electronic applications.

1. Introduction:

Transition metal oxide nanostructures have gained significant attention owing to their remarkable structural stability, tunable electrical properties, and broad applicability in catalysis, supercapacitors, gas sensors, and energy-storage devices [1–4]. Among various spinel oxides, $NiCo_2O_4$ has emerged as an important multifunctional material because of its mixed oxidation states and high electrochemical activity [5]. However, the relatively low intrinsic conductivity of pristine $NiCo_2O_4$ limits its practical applications in advanced electronic and electrochemical systems [6].

Elemental substitution has been widely adopted to enhance the electrical conductivity and dielectric beh-

avior of spinel oxides. Zn incorporation into the $NiCo_2O_4$ lattice modifies the electronic structure and promotes charge carrier mobility by influencing the hopping mechanism between Co^{2+}/Co^{3+} and Ni^{2+}/Ni^{3+} ions [7–9]. Zn-substituted nickel cobaltites have therefore attracted considerable interest due to their improved electrochemical stability, enhanced dielectric response, and superior conductivity [10–12].

In the present work, Zn-doped $NiCo_2O_4$ nanoparticles were synthesized using a microwave-assisted hydrothermal technique. Structural, chemical, and dielectric investigations were performed to evaluate the influence of Zn incorporation on the electrical transport properties and dielectric performance of the prepared nanoparticles.

2. Experimental

2.1. Synthesis of Anode Materials:

Analytical-grade nickel nitrate, cobalt nitrate, zinc nitrate trihydrate, and sodium hydroxide were used as precursor materials without additional purification. Stoichiometric quantities of the precursor salts were dissolved in double-distilled water and magnetically stirred to obtain a homogeneous solution.

The resulting solution was transferred into a microwave hydrothermal reactor and processed at 60 °C for 40 min. The obtained precipitate was repeatedly washed using deionized water and ethanol, followed by drying at 80 °C overnight. Finally, the dried powders were calcined at 600 °C for 4 h to obtain Zn-doped $NiCo_2O_4$ nanoparticles

2.2. Characterizations:

Structural characterization was performed using X-ray diffraction with Cu Kα radiation. FTIR spectra were recorded to identify vibrational modes and chemical bonding. XPS analysis was carried out to determine elemental composition and oxidation states. Dielectric measurements were conducted using an LCR meter over a wide frequency range at room temperature.

3. Results and discussions

3.1 XRD

The Fig.2 shows the XRD phase analysis of Zn doped $NiCo_2O4$.The crystallite phase information of the different samples of $NiZn_xCo_{2-x}O_4$ (x = 0.00, 0.02, 0.04,0.06,0.08 and 0.10) supported on NF is verified by XRD. The XRD spectra shown in Fig. confirm that the coprecipitation method results in a practically pure $NiCo_2O_4$ [17]. Spinel crystalline lattice. The crystallite is characterized by a face-centred cubic spinel lattice with a spatial group Fd3m. The unit cell dimension of the spinel structure a_0, was determined from the observed d-spacing for the planes by using the formula for a cubic lattice:

Sl.No	Zn Doping X=	Lattice Parameter $a = d\sqrt{(h^2+k^2+l^2)}$ A°	Crystal size <D> = 0.9 λ/β Cos θ nm	X- ray density ρ= ZM/Na3 (gr/cm³)
1	0.00	7.63	42.52	10.924
2	0.02	8.31	43.29	5.680
3	0.06	8.33	39.26	5.883
4	0.08	8.27	43.01	5.756
5	0.10	8.34	44.30	5.571

Table 1: The evaluated structural parameters verify the successful formation of phase-pure

polycrystalline Zn-doped $NiCo_2O_4$ nanoparticles with a well-defined cubic spinel lattice.

$a = d\sqrt{(h^2+k^2+l^2)}$ Å---------- (2)
where h, k and l are the Miller indices.
and calculated the parameters with the help of equation following equations:
The average Crystal size using Debye scherrer's formula,
$\langle D\rangle = 0.9\,\lambda/\beta \cos\theta$ nm ----- (2)
and the X-ray density,
$\rho = ZM/Na^3$ g/cm³ --------- (3)
The lattice constant values calculated for pure and Zn-doped $NiCo_2O_4$ samples are listed in Table 1. The obtained results closely match the standard value of 0.831 nm reported in the ICSD database (collection codes: 01-073-1704, 00-023-1390, and 01-076-1802), confirming the formation of the cubic spinel structure in Zn-doped $NiCo_2O_4$ nanoparticles.

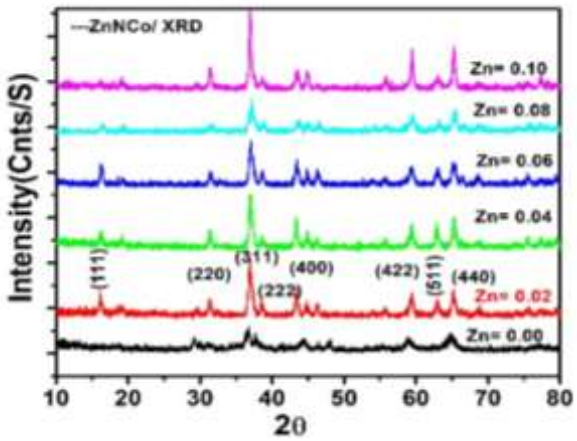

Fig. 1: XRD plot of pure and Zn doped $NiCo_2O_4$ NPs..

3.2. Fourier Transform Infrared Spectroscopy (FTIR):

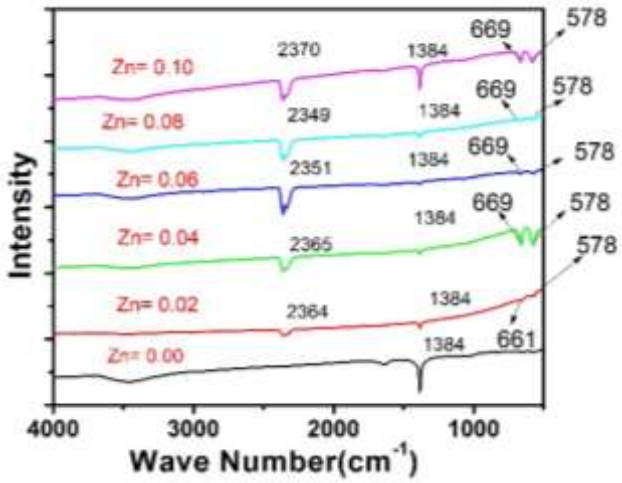

Fig. 2: Fourier Transform Infrared spectra of pure and Zn doped $NiCo_2O_4$ NPs.

FTIR spectra exhibited prominent absorption bands around 669 cm^{-1} and 578 cm^{-1}, corresponding to metal–oxygen stretching vibrations within tetrahedral and octahedral sites of the spinel lattice. The gradual reduction in peak intensity with increasing Zn content indicated lattice imperfections and oxygen vacancy formation.

3.2. XPS analysis:

To obtain more detailed information on the elemental composition and related oxidation states of the individual catalysts surfaces, XPS analysis was performed. The corresponding spectra are presented in Fig.5 (a-e).

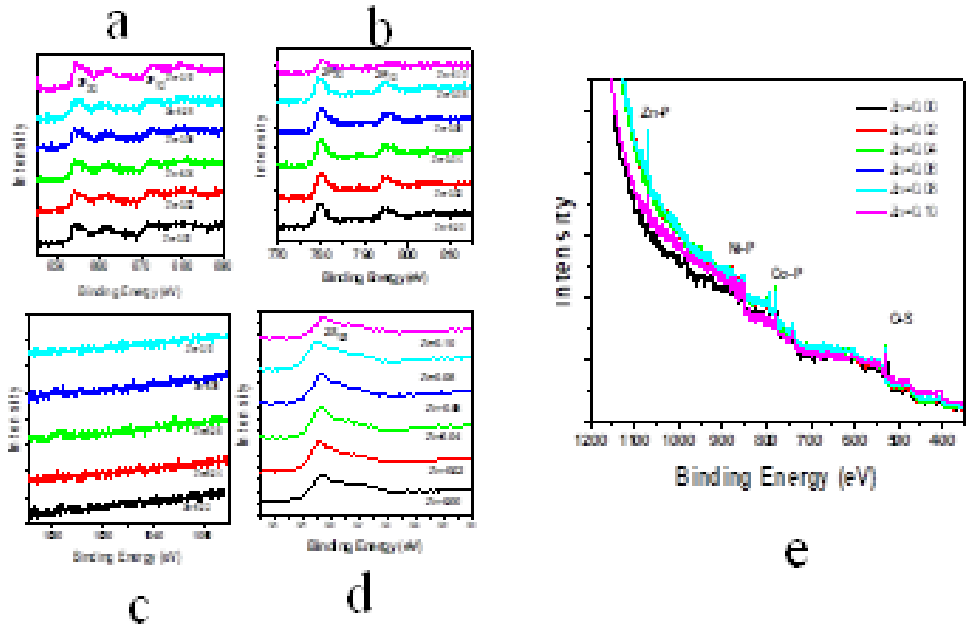

Fig.5:(a-e)-X-ray Photoelectron Spectroscopy (XPS) of $NiZn_xCo_{2-x}O_4$ showing the binding energy vs Intensity of Zn, Ni, Co, O and convoluted graph for x=0.00, 0.02, 0.06, 0.08 and 0.10.

Sl.No	Zn Doping X	Binding Energy(eV)						
		Co		Ni		Zn		O
		$2P_{3/2}$	$2P_{1/2}$	$2P_{3/2}$	$2P_{1/2}$	$2P_{3/2}$	$2P_{1/2}$	$2S_{1/2}$
1	X=0.00	854	872.37	854.95	872.42	--	--	530.06
2	X= 0.02	780.23	795.25	854.58	861.44	1021.70	1033.08	529.80
3	X= 0.06	780.25	795.39	854.80	861.62	1021.08	1033.88	529.80
4	X= 0.08	779.56	795.24	854.66	872.18	1020.64	1036.19	529.91
5	X= 0.10	780.62	795.47	855.32	861.52	1020.40	1030.43	530.18

Table 2: Tabulated the values of band gap energies of the compositions Zn, Co, Ni and O of their orbital states.

XPS studies further confirmed the coexistence of Ni^{2+}/Ni^{3+} and Co^{2+}/Co^{3+} oxidation states. The observed binding energy shifts with Zn incorporation verified the successful substitution of Zn ions and the resulting modification in the electronic structure.

4. Dielectric Properties

The dielectric properties of the copper-doped nickel cobaltite (ZnNCO) nano particles have been measured using the LCR meter. Pelletized samples were mounted in an impedance analyser to study their dielectric behaviour.

4.1 Dielectric Constant

The dielectric behaviour of $Ni_{1-x}Zn_xCo_2O_4$ (x = 0.0, 0.2, 0.4, 0.6, 0.8) was studied at RT using a dielectric analyser. The complex dielectric constant

$$\varepsilon^* = \varepsilon' + i\varepsilon''$$

is expressed in terms of the real part

$$\varepsilon' = \frac{C}{C_0} = \frac{Cd}{\varepsilon_0 A}$$

where C is the capacitance, d the pellet thickness, ε_0 the permittivity of free space, and A the cross sectional area of the pellet[18] .

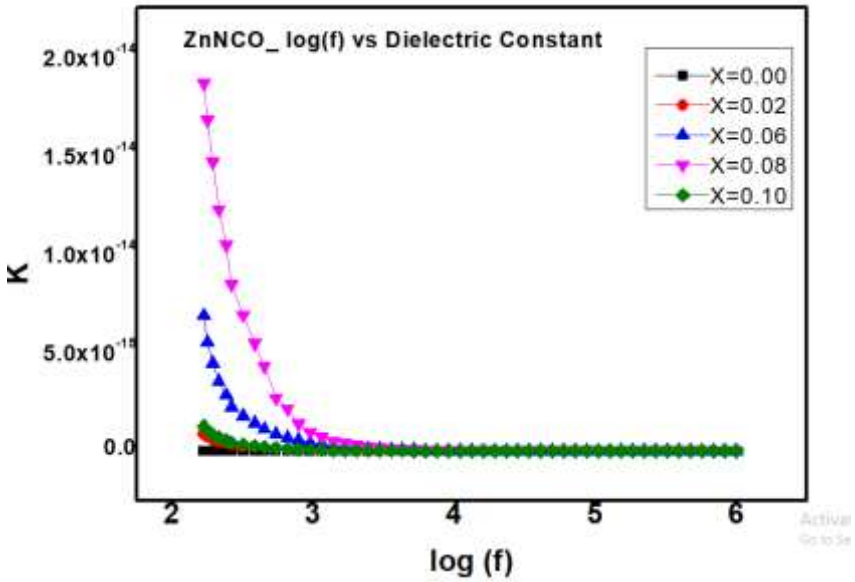

Fig.6: the Graph between log (f) Vs Dielectric constant for Zn doped $NiCo_2O_4$

The dielectric constant measured at room temperature showed high values at low frequencies and gradually decreased with increasing frequency. This behavior can be explained by the Maxwell–Wagner interfacial polarization model and Koop's phenomenological theory [18,21]. At lower frequencies, space-charge polarization dominates because charge carriers accumulate at grain boundaries. At higher frequencies, the dipoles fail to follow the rapidly varying electric field, resulting in reduced dielectric polarization.

4.2 Dielectric Loss

Dielectric loss quantifies energy dissipated as heat under an AC electric field. The loss tangent [19]

$$\tan\,\delta = \frac{\varepsilon''}{\varepsilon'}$$

Exhibits a maximum at low frequencies for x = 0.0 and decreases with increasing frequency. Zn substitution reducestan δ, with further decrease upon increasing Zn content, indicating lower energy loss and improved energy storage capability. This behaviour is associated with relaxation peaks that

occur when the applied frequency approaches the hopping frequency of charge carriers, where energy dissipation is minimized and the dielectric loss is reduced.

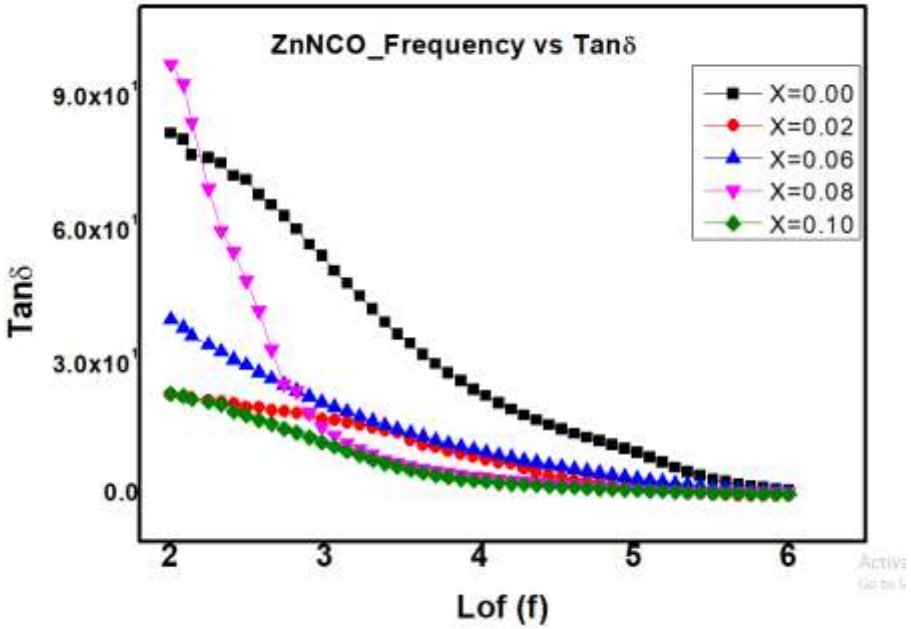

Fig.7: the Graph between log (f) Vs tan δ for Zn doped $NiCo_2O_4$

The dielectric loss also decreased with increasing frequency, indicating reduced energy dissipation and improved dielectric stability at higher frequencies. Zn substitution effectively reduced dielectric loss due to suppression of interfacial polarization and improved charge transport behavior.

The rapid decrease in tan δ at higher frequencies confirms the suppression of interfacial polarization and domain wall motion. Overall, Zn doping effectively reduces dielectric loss, making the material more suitable for high-frequency dielectric and electronic applications.

4.3 Conductivity

Figure 8 shows the variation of AC conductivity (σ_ac) with frequency for pure and Zn-doped $NiCo_2O_4$ (ZnNCO) samples. The AC conductivity increases with increasing frequency for all compositions, indicating the typical frequency-dependent conduction behavior of ferrite materials. The conductivity was calculated using the relation:

$$\sigma_{ac} = 2\pi f \varepsilon_0 \varepsilon' \tan \delta$$

Where ε' is the real dielectric constant, f the frequency, and ε_0 the permittivity of free space .

.

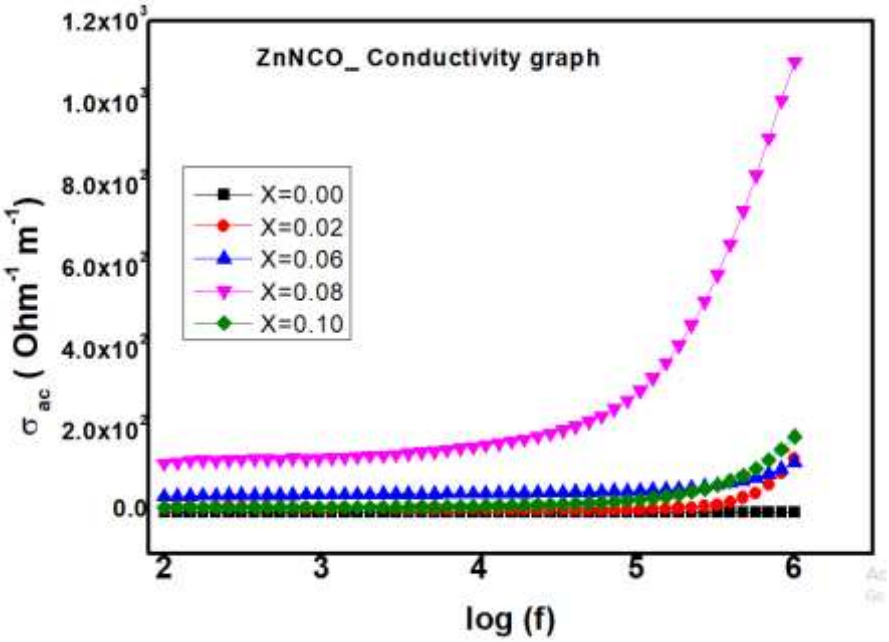

Fig.8: the Graph between log (f) Vs Conductivity for Zn doped $NiCo_2O_4$

AC conductivity measured at room temperature increased progressively with frequency for all compositions. The enhancement in conductivity was attributed to electron hopping between mixed valence ions and reduced grain boundary resistance. The x = 0.08 composition exhibited the highest conductivity, suggesting optimum Zn incorporation for enhanced electrical transport.

5. Conclusions

Zn-doped $NiCo_2O_4$ nanoparticles were successfully synthesized using a microwave-assisted hydrothermal technique. Structural studies confirmed the formation of a phase-pure cubic spinel structure. FTIR and XPS analyses verified the successful incorporation of Zn ions into the $NiCo_2O_4$ lattice. Dielectric studies performed at room temperature demonstrated strong frequency-dependent behavior, where the dielectric constant and dielectric loss decreased with increasing frequency, while AC conductivity increased significantly. Zn incorporation enhanced the electrical conductivity and dielectric performance of $NiCo_2O_4$ nanoparticles. Among the investigated compositions, the x = 0.08 sample exhibited optimum electrical transport characteristics, making it a promising material for high-frequency electronic and energy-storage applications.

References

1. M.M.M. Mostafa, W. Bajafar, L. Gu, K. Narasimharao, M. Abdel Salam, A. Alshehri, N.H. Khdary, S. Al-Faifi, A.D. Chowdhury, Electrochemical Characteristics of Nanosized Cu, Ni, and Zn Cobaltite Spinel Materials, Catalysts. 12 (2022) 893, https://doi.org/10.3390/catal12080893.
2. F. Lu, M. Zhou, W. Li, Q. Weng, C. Li, Y. Xue, X. Jiang, X. Zeng, Y. Bando, D. Golberg, Engineering sulfur vacancies and impurities in NiCo2S4 nanostructures toward optimal supercapacitive performance, Nano Energy 26 (2016) 313–323, https://doi.org/10.1016/j.nanoen.2016.05.042.

3. Y. Guo, L. Yu, C.-Y. Wang, Z. Lin, X.W.(David) Lou, , Hierarchical Tubular Structures Composed of Mn-Based Mixed Metal Oxide Nanoflakes with Enhanced Electrochemical Properties, Adv. Funct. Mater. 25 (2015) 5184–5189, https://doi. org/10.1002/adfm.201501974.
4. X. Xie, Z. Ao, D. Su, J. Zhang, G. Wang, MoS2/Graphene Composite Anodes with Enhanced Performance for Sodium-Ion Batteries: the Role of the Two-Dimensional Heterointerface, Adv. Funct. Mater. 25 (2015) 1393–1403, https://doi.org/ 10.1002/adfm.201404078.
5. M. Guo, J. Balamurugan, X. Li, N.H. Kim, J.H. Lee, Hierarchical 3D Cobalt-Doped Fe3O4 Nanospheres@NG Hybrid as an Advanced Anode Material for High- Performance Asymmetric Supercapacitors, Small. 13 (2017) 1701275, https://doi. org/10.1002/smll.201701275.
6. W. Lu, Z. Yuan, C. Xu, J. Ning, Y. Zhong, Z. Zhang, Y. Hu, Construction of mesoporous Cu-doped Co9S8 rectangular nanotube arrays for high energy density all-solid-state asymmetric supercapacitors, J. Mater. Chem. A 7 (2019) 5333–5343, https://doi.org/10.1039/C8TA10998B.
7. X. Han, L. Song, J. Ding, L. Hu, C. Xu, Y. Wang, Design and preparation of Cu-doped NiCo2O4 nanosheets with intrinsic porosities for symmetric supercapacitors, Mater. Lett. 278 (2020) 128400, https://doi.org/10.1016/j.matlet.2020.128400.
8. H. Park, B.H. Park, J. Choi, S. Kim, T. Kim, Y.-S. Youn, N. Son, J.H. Kim, M. Kang, Enhanced Electrochemical Properties and OER Performances by Cu Substitution in NiCo2O4 Spinel Structure, Nanomaterials 10 (2020) 1727, https://doi.org/ 10.3390/nano10091727.
9. X. Ge, Y. Liu, F.W.T. Goh, T.S.A. Hor, Y. Zong, P. Xiao, Z. Zhang, S.H. Lim, B. Li, X. Wang, Z. Liu, Dual-Phase Spinel MnCo2O4 and Spinel MnCo2O4/Nanocarbon Hybrids for Electrocatalytic Oxygen Reduction and Evolution, ACS Appl. Mater. Interfaces 6 (2014) 12684–12691, https://doi.org/10.1021/am502675c.
10. R. Yang, J. Yesuraj, J. Kim, K. Kim, Spinel-structured CuCo2O4 with a mixed 1D/2D morphology for asymmetric supercapacitor and oxygen evolution electrocatalyst applications, Electrochim. Acta 437 (2023) 141507, https://doi.org/10.1016/j. electacta.2022.141507.
11. H. Wang, X. Song, H. Wang, K. Bi, C. Liang, S. Lin, R. Zhang, Y. Du, J. Liu, D. Fan, Y. Wang, M. Lei, Synthesis of hollow porous ZnCo2O4 microspheres as high-performance oxygen reduction reaction electrocatalyst, Int. J. Hydrogen. Energy 41 (2016) 13024–13031, https://doi.org/10.1016/j.ijhydene.2016.05.046.
12. D.S. Nair, A. Anil, L. Elias, N. Satyanarayana, H.K. Holla, S.M.A. Shibli, Tuning of physicochemical and electronic characteristics of Cu-doped NiCo2O4 ternary inverse spinel oxides for effective electrocatalytic hydrogen evolution reaction, Int. J. Hydrogen. Energy 62 (2024) 162–171, https://doi.org/10.1016/j. ijhydene.2024.03.031.
13. A. Naz, I. Bibi, F. Majid, A. Dahshan, K. Jilani, B. Taj, A. Ghafoor, Z. Nazeer, F. M. Alzahrani, M. Iqbal, Cu and Fe doped NiCo2O4/g-C3N4 nanocomposite ferroelectric, magnetic, dielectric and optical properties: visible light-driven photocatalytic degradation of RhB and CR dyes, Diam. Relat. Mater. 141 (2024) 110592, https://doi.org/10.1016/j.diamond.2023.110592.
14. O.M. Ozkendir, E. Cengiz, M. Mirzaei, I.H. Karahan, R. ¨Ozdemir, W. Klysubun, Electronic structure study of the bimetallic Cu1-xZnx alloy thin films, Materials Technology 33 (2018) 193–197, https://doi.org/10.1080/ 10667857.2017.1391932.
15. T.R. Silva, R.A. Raimundo, V.D. Silva, J.R.D. Santos, L.S. Ferreira, A.J.M. Araújo, F. J.A. Loureiro, F.F. da Silva, D.P. Fagg, D.A. Macedo, Green synthesis of MnCo2O4 nanoparticles grown on 3D nickel foam as a self-supported electrode for oxygen evolution reaction, Colloids and Surfaces

A: Physicochemical and Engineering Aspects 672 (2023) 131626, https://doi.org/10.1016/j.colsurfa.2023.131626.

16. R. Nakhowong, R. Chueachot, Synthesis and magnetic properties of copper cobaltite (CuCo2O4) fibers by electrospinning, J. Alloys. Compd. 715 (2017) 390–396, https://doi.org/10.1016/j.jallcom.2017.04.323.
17. Liu, L.; Wang, J.; Hou, Y.; Chen, J.; Liu, H.K.; Wang, J.; Wu, Y. Self-Assembled 3D Foam-Like NiCo2O4 as Efficient Catalyst for Lithium Oxygen Batteries. Small 2016, 12, 602–611.
18. A. Garg, L.K. Parmar, T. Garg, H.S. Dager, P. Bhardwaj, A. Yadav, Structural analysis and dielectric behavior of low-temperature synthesized nickel cobaltite, Chemical Physics Impact 8 (2024) 100457, https://doi.org/10.1016/j. chphi.2024.100457.
19. P.B. Belavi, G.N. Chavan, L.R. Naik, R. Somashekar, R.K. Kotnala, Structural, electrical and magnetic properties of cadmium substituted nickel–copper ferrites, Mater. Chem. Phys. 132 (2012) 138–144, https://doi.org/10.1016/j. matchemphys.2011.11.009.
20. V.N. Dhage, M.L. Mane, S.B. Rathod, S.M. Rathod, K.M. Jadhav, Electric, dielectric and AC electrical conductivity study of Al3+ substituted barium hexaferrite nanoparticles synthesized by Sol-gel auto-combustion technique, Materials Today: Proceedings 47 (2021) 1982–1987, https://doi.org/10.1016/j.matpr.2021.04.119.
21. C.G. Koops, On the Dispersion of Resistivity and Dielectric Constant of Some Semiconductors at Audiofrequencies, Phys. Rev. 83 (1951) 121–124, https://doi. org/10.1103/PhysRev.83.121. [31] A. Yadav, P. Choudhary, P. Saxena,
22. A. Yadav, P. Choudhary, P. Saxena, V.N. Rai, A. Mishra, Spectroscopic analysis and temperature-dependent dielectric properties of bulk Ni–Zn ceramics, J. Adv. Dielect. 09 (2019) 1950014, https://doi.org/10.1142/S2010135X19500140